THE JOURNAL OF PHYSICAL CHEMISTRY A

ARTICLE

pubs.acs.org/JPCA

Laboratory Investigation on the Role of Organics in Atmospheric Nanoparticle Growth

Lin Wang,[†,‡] Wen Xu,[†] Alexei F. Khalizov,[†] Jun Zheng,[†] Chong Qiu,[†] and Renyi Zhang*[,†,‡]

[†]Department of Atmospheric Sciences and Department of Chemistry, Texas A&M University, College Station, Texas 77843, United States

[‡]Department of Environmental Science & Engineering and Institute of Global Environment Change Research, Fudan University, 220 Handan Rd., Shanghai 200433, P. R. China

ABSTRACT: The uptake of organic vapors by 4−20 nm H_2SO_4 particles has been investigated to assess the role of organics in atmospheric nanoparticle growth. Sulfuric acid nanoparticles are generated from homogeneous binary nucleation of H_2SO_4 and H_2O vapors in a laminar flow chamber. The growth factor of H_2SO_4 nanoparticles exposed to methyglyoxal, ethanol, 1-butanol, 1-heptanol, and 1-decanol is measured using a nanotandem differential mobility analyzer (nano-TDMA). The measured growth factor is close to unity when nanoparticles are exposed to methylglyoxal, ethanol, 1-butanol, 1-heptanol, and 1-decanol, indicating no apparent growth within the experimental uncertainty. In addition, spectroscopic evolution of functional groups in H_2SO_4 particles of ~40 nm diameter size, deposited on ZnSe crystal and subsequently exposed to glyoxal and 2,4-hexadienal, is studied using attenuated total reflection−Fourier transform infrared spectroscopy (ATR-FT-IR). The ATR-FT-IR measurements present the first spectroscopic signatures of high molecular weight aldol and oligomer products and show that polymerization and oligomerization reactions are partially reversible. The implications of the present results to nanoparticle growth in the atmosphere are discussed.

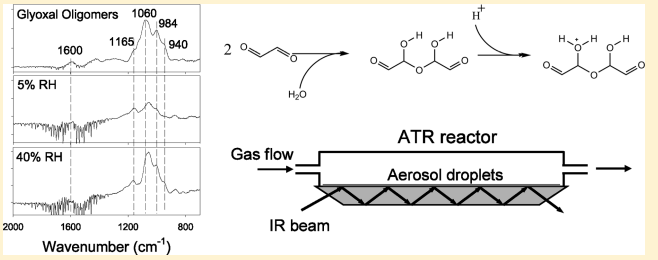

1. INTRODUCTION

Aerosol nucleation events have been frequently observed in urban and rural sites around the world.[1,2] New particle formation occurs in two distinct stages, i.e., nucleation to form the critical nucleus and subsequent growth of the critical nucleus to detectable particles (1.5−3 nm or larger).[3] Several mechanisms have been proposed to explain aerosol nucleation in the atmosphere, including binary nucleation of sulfuric acid and water,[4,5] ternary nucleation of sulfuric acid, ammonia, and water,[6,7] ion-induced nucleation,[8,9] and nucleation assisted by organic acids.[10,11] The fate of freshly nucleated particles is determined by the competition between scavenging by pre-existing particles and growth to larger aerosol particles and cloud condensation nuclei (CCN), which directly and indirectly alter radiative balance of the earth−atmosphere system to impact cloud formation and climate, pose negative effects on human health, and affect atmospheric multiphase chemical processes.[12−14]

Typical growth rates during new particle formation events are 1−20 nm h^{-1} in mid-latitudes, depending on the temperature and concentration of condensable vapors.[1,2] Simultaneous measurements of nanoparticle growth rates and gas-phase H_2SO_4 concentrations show that H_2SO_4 typically accounts for 5−50% of the observed growth.[15,16] This implies that other species, including organics, also contribute to the growth of nucleation mode particles (<20 nm). However, particles in the nucleation mode are subject to a large curvature (Kelvin) effect.[17] The considerably elevated equilibrium vapor pressure over freshly nucleated particles implies that condensation and partitioning of organics are highly hindered by the Kelvin barrier.

It has been hypothesized that heterogeneous reactions can be responsible for growth of nucleation mode particles.[18] Recent progress has been made to assess the role of organics in atmospheric nanoparticle growth. A laboratory study has shown that heterogeneous reactions of glyoxal, 2,4-hexadienal, and trimethylamine lead to the growth of nanoparticles smaller than 20 nm.[19] In addition, a number of field observations have suggested that organics play a role in nanoparticle growth.[15,16,20−25] Measurements of nanoparticle growth rates revealed a clear annual cycle with the highest value in summer and the lowest value in winter, indicative of a correlation between photochemistry and the growth of nucleation mode particles.[20] Also, observations of the water affinity of 2−9 nm particles showed that freshly nucleated particles are less hygroscopic than pure sulfuric acid or ammonium sulfate, implying that less hygroscopic compounds, presumably organics, are present,[21] although little information on the speciation of the individual organics is available. Direct measurements using thermal desorption chemical ionization mass spectrometer (TD-CIMS) demonstrated the presence of various organic ions in ambient particles of 10−33 nm diameter.[22] The presence of aminium salts in newly formed

Received: December 22, 2010
Revised: July 11, 2011
Published: July 12, 2011

dx.doi.org/10.1021/jp1121855 | J. Phys. Chem. A 2011, 115, 8940–8947

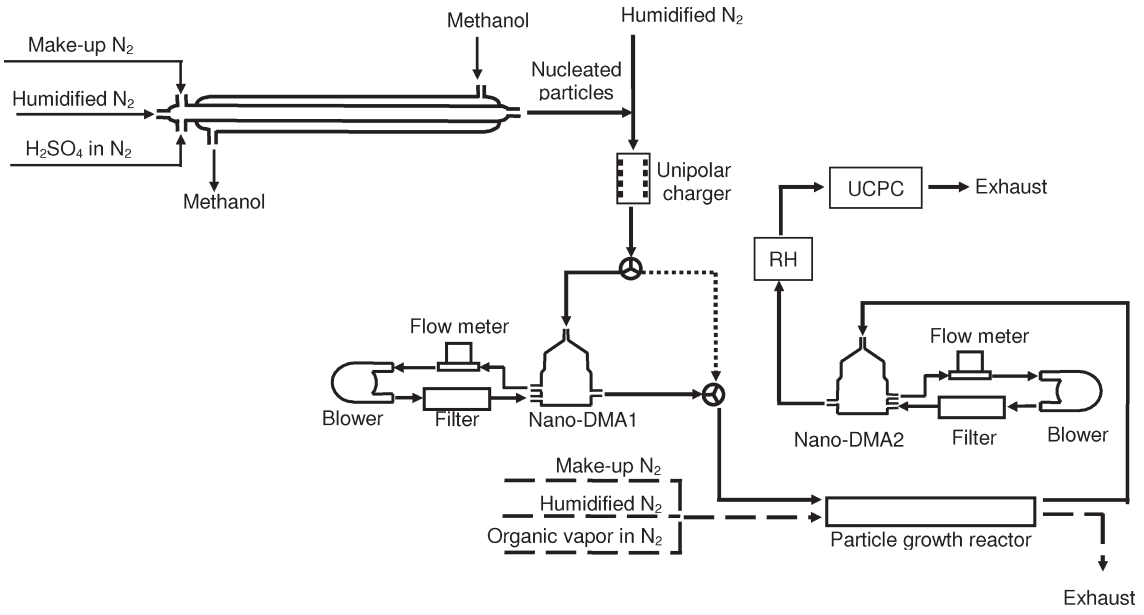

Figure 1. Schematic representation of the apparatus for measuring aerosol growth using nano-TDMA.

atmospheric particles has been confirmed by analyzing particle chemical compositions,[23] consistent with the results from the laboratory studies.[19,26] The presence of nonvolatile residuals by volatility-tandem differential mobility analyzer (TDMA)[15] and volatility-scanning mobility particle sizer (SMPS)[24] can potentially be explained by the formation of polymers and oligimers because aminium salts decompose at ~150 °C,[23] much lower than the temperature of the thermodenuder used in the volatility studies.

In this paper, we report laboratory experiments to evaluate the contribution of heterogeneous reactions of atmospherically relevant organic compounds to H_2SO_4 nanoparticle growth, including glyoxal, methylglyoxal, 2,4-hexadienal, ethanol, 1-butanol, 1-heptanol, and 1-decanol. Those organic compounds are selected to represent diverse products of photochemical oxidation of volatile organic compounds from natural and anthropogenic sources.[27−29] Two analytical techniques are used to quantify the growth of nanoparticles exposed to organic vapors and to elucidate the underlying mechanisms of the heterogeneous reactions, including nano-TDMA and attenuated total reflection−Fourier transform infrared spectroscopy (ATR-FT-IR). This work extends over our previous work[19] by including additional species and spectroscopic data to assess the contributions of organics to nanoparticle growth.

2. EXPERIMENTAL SECTION

Nanoparticles (≤20 nm) were generated from the H_2SO_4−H_2O binary nucleation. The growth factor of nanoparticles upon exposure to organic vapors was measured using nano-TDMA. Also, sulfuric acid particles of ~40 nm diameter size were generated by an atomizer, deposited onto a ZnSe crystal, and exposed to organic vapors to study spectroscopic evolution of functional groups by ATR-FT-IR.

H_2SO_4 (95−98%, ACS reagent grade), 2,4-hexadienal ($CH_3CH{=}CHCH{=}CHCHO$, 95%), ethanol (CH_3CH_2OH, >99.5%), 1-butanol ($CH_3(CH_2)_2CH_2OH$, >99.9%), 1-heptanol ($CH_3(CH_2)_5CH_2OH$, >99.5%), and 1-decanol ($CH_3(CH_2)_8CH_2OH$, >99.5%) were purchased from Sigma-Aldrich and used as received without further purification. Deionized water (18 mΩ·cm) was generated using a Barnstead E-Pure water system. Glyoxal monomer (CHOCHO) was synthesized by heating equal amounts of glyoxal trimer dihydrate (>97%, Sigma-Aldrich) and P_2O_5 (Sigma-Aldrich) to 423 K, whereas methylglyoxal monomer (CH_3COCHO) was synthesized from its aqueous solution (40%, Sigma-Aldrich).[30] The gas phase product was continuously pumped through a P_2O_5 trap to remove water vapor and then collected at dry ice−acetone temperature (−78 °C). The collected yellow glyoxal crystals and green-yellowish methylglyoxal crystals, respectively, were stored in dry ice−acetone bath (−78 °C) and kept in a 37 wt % $CaCl_2$ water solution/liquid nitrogen bath (−51 °C) when in use. The purity of glyoxal and methylglyoxal was checked by infrared spectroscopy, and only freshly synthesized glyoxal and methylglyoxal were used for ~48 h before they became hydrolyzed.

2.1. Generation of Nanoparticles. Nanoparticles were generated in a laminar flow chamber. A description of the laminar flow nucleation chamber has been provided previously.[11,19] Gaseous sulfuric acid was introduced to the nucleation chamber by passing a small flow of nitrogen through a bubbler containing concentrated liquid sulfuric acid, and the inlet of the bubbler was heated to ~363 K to reduce the wall loss of sulfuric acid. The bubbler was immersed in a water bath regulated at 313−333 K. Water vapor was admitted to the nucleation chamber by bubbling a flow of nitrogen through a Pyrex bubbler containing deionized water. The humidity was determined using a hygrometer by measuring the dew point of water vapor. An ion drift−chemical ionization mass spectrometer (ID-CIMS) was used to monitor the concentrations of gas-phase sulfuric acid.[31,32]

2.2. Measurements of Nanoparticle Growth. Experiments of nanoparticle growth were carried out using a combination of a unipolar aerosol charger, a growth reactor, and a nano-TDMA, as depicted in Figure 1. The nano-TDMA system, comprising of two differential mobility analyzers (DMA 3085, TSI) and an ultrafine condensation particle counter (CPC 3025A, TSI), was developed to measure the nanoparticle concentration and size distribution. A program written in LabVIEW software was used

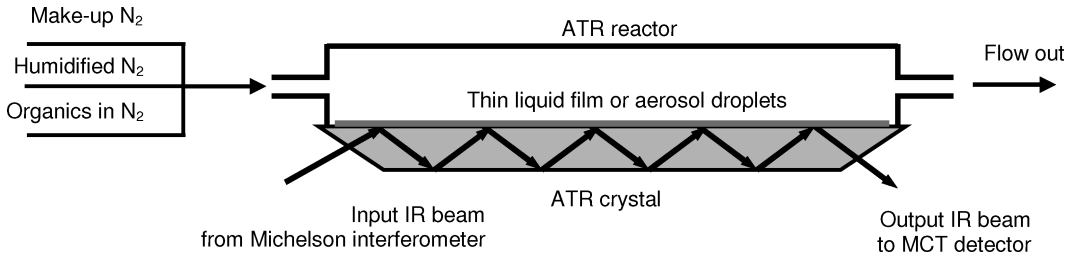

Figure 2. Schematic representation of ATR-FT-IR setup.

to control the system through National Instruments DAQ interface cards. During the growth experiments, the aerosol sample flow was passed through a route as labeled by the solid line in Figure 1. The aerosol sample flow rate through both DMAs and CPC was kept at 1.5 slpm, and the sheath flow rate for DMAs was maintained at 15 slpm.

The unipolar aerosol charger minimized neutralization of oppositely charged particles.[33] In our experiments, nanoparticles were charged by exposing the aerosol flow to α particles emitted from radioactive ^{210}Po foils and subsequently passed through a 20 cm electric field of 2.5 V cm^{-1} to minimize neutralization of oppositely charged particles. The overall charging efficiency for 2−13 nm particles was ∼10%, about a factor of 5 larger than a traditional bipolar charger.

The aerosol flow from the nucleation chamber was mixed with a humidified nitrogen flow to adjust the relative humidity (RH) with a typical uncertainty of 2%. Sulfuric acid particles were charged by the unipolar charger and size-selected using the first nano-DMA. Subsequently, monodisperse particles were introduced into a particle growth reactor (1.5 m length × 2.54 cm i.d.), where they were exposed to organic vapors. The organic vapor was introduced into the growth reactor at a flow rate of 450 mL min^{-1} and at a relative humidity identical to the sample flow. A flow of 450 mL min^{-1} was removed at the end of the growth reactor using a critical orifice followed by a pump to keep the aerosol flow rate. The time scale of exposure of particles to organic vapors in the growth reactor was about 30 s. The second nano-DMA interfaced to the CPC was used to measure the aerosol size distribution. The growth factor is expressed as D_p/D_0, where D_p is the aerosol diameter after organic exposure and D_0 is the initial aerosol diameter. After each experiment, the tubing and the growth reactor were thoroughly washed and heated at 150 °C in an oven, and the filter was dissembled and flushed with dry nitrogen at 75 °C overnight to remove organic residues.

The concentration of methylglyoxal was measured to be 9 × 10^{13} molecules cm^{-3} by a Perkin-Elmer 552 UV−vis spectrophotometer. The concentrations of ethanol, 1-butanol, 1-heptanol, and 1-decanol were estimated to be 2 × 10^{16}, 2 × 10^{15}, 6 × 10^{13}, and 4 × 10^{12} molecules cm^{-3}, respectively, using the volumetric flow ratios and their saturation vapor pressures, and validated by a proton transfer reaction−mass spectrometer (PTR-MS).[34] The concentrations of the organic vapors employed were selected to achieve a measurable growth factor because of a shorter reaction time in our experiments.[19]

2.3. Composition Analysis by ATR-FT-IR. The spectroscopic evolution of chemical species of deposited sulfuric acid particles by heterogeneous uptake of organic vapors was studied by monitoring the ATR-FT-IR spectra, using a Nicolet Magna 560 spectrometer equipped with an MCT detector. Sulfuric acid particles of ∼40 nm diameter size were produced by a TSI 3076 constant output atomizer and deposited onto a ZnSe crystal (Pike Technologies). The total mass of deposited sulfuric acid particles was ∼3 mg, and the thickness of the H_2SO_4 droplet layer was less than 2 μm, i.e., the penetration depth of infrared over the 400−4000 cm^{-1} region. Background spectra were recorded after the deposition of sulfuric acid particles. Subsequently, a flow of nitrogen carrying the organic vapor was passed through a temperature and RH controlled reactor built on the top of the ATR crystal, as shown in Figure 2. ATR-FT-IR spectra were recorded at various time intervals to monitor the formation of functional groups. Typically, 60 scans at a resolution of 4 cm^{-1} over the wavenumber range from 4000 to 600 cm^{-1} were averaged to generate the spectra. The exposure to organic vapors was terminated at 60 min, after which monitoring of spectra variation was continued for another 60 min. The organic concentration at the entrance of the ZnSe reactor was measured to be 3.6 × 10^{14} molecules cm^{-3} for 2,4-hexadienal by PTR-MS and 2.8 × 10^{13} molecules cm^{-3} for glyoxal by the Perkin-Elmer 552 UV−vis spectrophotometer.

3. RESULTS

3.1. Nanoparticle Growth by Heterogeneous Reactions of Organic Vapors. The measured growth factors, D_p/D_0, of H_2SO_4 nanoparticles exposed to organic vapors are summarized in Table 1 at various RH and particle sizes. The acidity of H_2SO_4 nanoparticles is regulated by RH and particle size, i.e., to be lower at higher RH for a given particle size but higher at smaller particle size for a given RH. We estimate that composition of nanoparticles ranges from 40 to 80 wt % H_2SO_4 in the present work. Table 1 indicates that the measured growth factor is between 0.99 and 1.02 when nanoparticles are exposed to methylglyoxal, ethanol, 1-butanol, 1-heptanol, and 1-decanol, independent of particle acidity and size. Considering that the systematic error with two standard deviations of the measurements (2σ) is 0.01−0.02, the results indicate negligible growth within the experimental uncertainty when nanoparticles are exposed to methylglyoxal, ethanol, 1-butanol, 1-heptanol, and 1-decanol. Also shown in Table 1 for comparison are previously reported growth factors for glyoxal, 2,4-hexadienal, and trimethylamine: the growth factor increases noticeably with RH for glyoxal and slightly trimethylamine but decreases with for 2,4-hexadienal; for all three species the growth factor increases with the particle size.[19]

For comparable acidity, the observation of negligible growth of H_2SO_4 nanoparticles exposed to methylglyoxal, ethanol, 1-butanol, 1-heptanol, and 1-decanol is distinct from previously measured uptake using bulk H_2SO_4 solutions. For methylglyoxal, the previous results of the heterogeneous chemistry of methylglyoxal

Table 1. Measured Nanoparticle Growth Factors (D_p/D_0);[a] Also Shown for Comparison Are Previously Reported Growth Factors for Glyoxal, 2,4-Hexadienal, and Trimethylamine[19]

		growth factor D_p/D_0					
organics	relative humidity (%)	4 nm	6 nm	8 nm	10 nm	15 nm	20 nm
glyoxal[b]	7	1.02 ± 0.02			1.22 ± 0.03	1.46 ± 0.03	1.53 ± 0.02
	20	1.02 ± 0.01			1.28 ± 0.03	1.64 ± 0.04	1.93 ± 0.04
methylglyoxal	6	1.01 ± 0.02	0.99 ± 0.01		1.01 ± 0.01		1.01 ± 0.01
	20	1.01 ± 0.02	1.02 ± 0.01		1.02 ± 0.01		1.01 ± 0.01
	50		1.01 ± 0.01		1.01 ± 0.01		0.99 ± 0.01
2,4-hexadienal[b]	7	1.02 ± 0.02	1.02 ± 0.02	1.05 ± 0.02	1.08 ± 0.02	1.10 ± 0.03	1.13 ± 0.02
	12	1.02 ± 0.02	1.02 ± 0.02	1.03 ± 0.02	1.04 ± 0.02	1.08 ± 0.02	1.09 ± 0.03
	20	1.01 ± 0.01	1.01 ± 0.01	1.01 ± 0.01	1.01 ± 0.01	1.01 ± 0.01	1.01 ± 0.01
trimethylamine[b]	6	1.10 ± 0.01	1.12 ± 0.01		1.18 ± 0.01		1.18 ± 0.01
	45	1.12 ± 0.02	1.18 ± 0.01		1.19 ± 0.01		1.23 ± 0.01
ethanol	6	1.01 ± 0.01			1.00 ± 0.01		1.00 ± 0.01
1-butanol	3	1.02 ± 0.02			1.01 ± 0.01		1.01 ± 0.01
	7	1.02 ± 0.02			1.00 ± 0.01		1.00 ± 0.01
	15	1.01 ± 0.02			1.01 ± 0.01		1.00 ± 0.01
1-heptanol	6	1.00 ± 0.01			1.00 ± 0.01		1.00 ± 0.01
1-decanol	6	1.00 ± 0.01			1.00 ± 0.01		1.01 ± 0.01

[a] Each point corresponds to at least two separate exposure experiments, and for each exposure experiment nine measurements of growth factor were carried out. The error represents two standard deviations of all measurements (2σ). [b] Values as previously reported.[19]

with bulk liquid H_2SO_4 surfaces show an uptake that is dependent on acidity.[30] For 1-butanol and 1-decanol, the uptake on bulk liquid H_2SO_4 surfaces exhibits two distinct types of behaviors, i.e., partially irreversible vs totally irreversible, depending on the acid concentration and temperature.[35] It is also interesting to note that a large growth factor is measured for glyoxal on particles larger than 4 nm,[19] in contrast to that measured for methylglyoxal. Furthermore, it is clear that interference because of evaporation or condensation of other species, including sulfuric acid, in nanoparticle growth is minimal in our experiments, evident from the measured unity growth factor when nanoparticles are exposed to methylglyoxal, ethanol, 1-butanol, 1-heptanol, and 1-decanol.

3.2. Spectroscopic Studies by ATR-FT-IR. Since our present results demonstrate negligible growth of H_2SO_4 nanoparticles exposed to alcohols and methylglyoxal, we only carried out the ATR-FT-IR study of the spectroscopic evolution of function groups observed in deposited sulfuric acid particles by uptake of 2,4-hexadienal and glyoxal, for which noticeable growth of nanoparticles has been previously reported.[19] Figures 3 and 4 show the spectra obtained upon exposure of 2,4-hexadienal and glyoxal, respectively. The background spectra were collected after deposition of H_2SO_4 particles on the ATR cell, and spectra b−d in both figures represent changes in the spectra after the organic exposure.

Figure 3a represents the spectra of 2,4-hexadienal standard in liquid phase from the NIST Chemistry WebBook.[36] The spectra are characterized with carbonyl stretch (1690 cm^{-1}), alkenyl double bond stretch (1643 cm^{-1}), primary C−H bend (1452 cm^{-1}), and alkenyl C−H out-of-plane bend (1165, 1119, 1082, 1012, and 987 cm^{-1}).[37] The other three traces in Figure 3b−d correspond to ATR-FT-IR spectra of deposited H_2SO_4 particles upon exposure to 2,4-hexadienal at different relative humidity. In these three spectra, the carbonyl stretch (C═O) comprises a major absorption feature (∼1670 cm^{-1}) and a minor absorption feature (1690 cm^{-1}). The band at 1690 cm^{-1} indicates that the Henry's law governs the uptake of 2,4-hexadienal monomers. On the other hand, the formation of aldol products from 2,4-hexadienal monomers results in a carbonyl stretch at a lower frequency (∼1670 cm^{-1}), corresponding to a reduced force constant of the harmonic oscillation, because hydrogen bonding between the hydrogen atom in the OH group of the aldol and the oxygen atom in the C═O group of the aldol lengthens the C═O bond distance and leads to more a single-bond character (Scheme 1a).[37,38] Furthermore, the ratio of the carbonyl stretch (C═O stretch) at ∼1670 cm^{-1} to the alkenyl double bond stretch at 1643 cm^{-1} is significantly lower in the uptake experiments than that of the 2,4-hexadienal standard, consistent with the aldol condensation reaction mechanism where one carbonyl group is transformed into one hydroxyl group.[39] The 800−1200 cm^{-1} region is characterized with the appearance of new features such as C−OH stretch. The 3600−3650 cm^{-1} region for the O−H bond is not shown since during the experiments there was a slight variation in RH, which interfered with the absorbance in this wavenumber range.

The relative intensity of the three spectra upon 2,4-hexadienal exposures at different relative humidity reflects the dependence of the previously measured growth factor with RH, i.e., larger growth factor at lower relative humidity.[19] Note that uptake of 2,4-hexadienal was observed at 60% RH in the ATR-FT-IR experiments, whereas no particle growth is measured for H_2SO_4 particles at this high RH in the previous nano-TDMA experiments.[19] This discrepancy is likely attributed to the curvature effect, i.e., Kelvin effect, since a bulk H_2SO_4 droplet layer is used in the ATR-FT-IR experiments while nanoparticles are studied in the nano-TDMA experiments. The uptake of 2,4-hexadienal reached equilibrium after ∼30 min exposure since the intensity of relevant IR peaks did not increase further (not shown in Figure 3). After the exposure to 2,4-hexadienal was terminated but the total N_2 flow and relative humidity were kept as the same,

dx.doi.org/10.1021/jp1121855 |J. Phys. Chem. A 2011, 115, 8940–8947

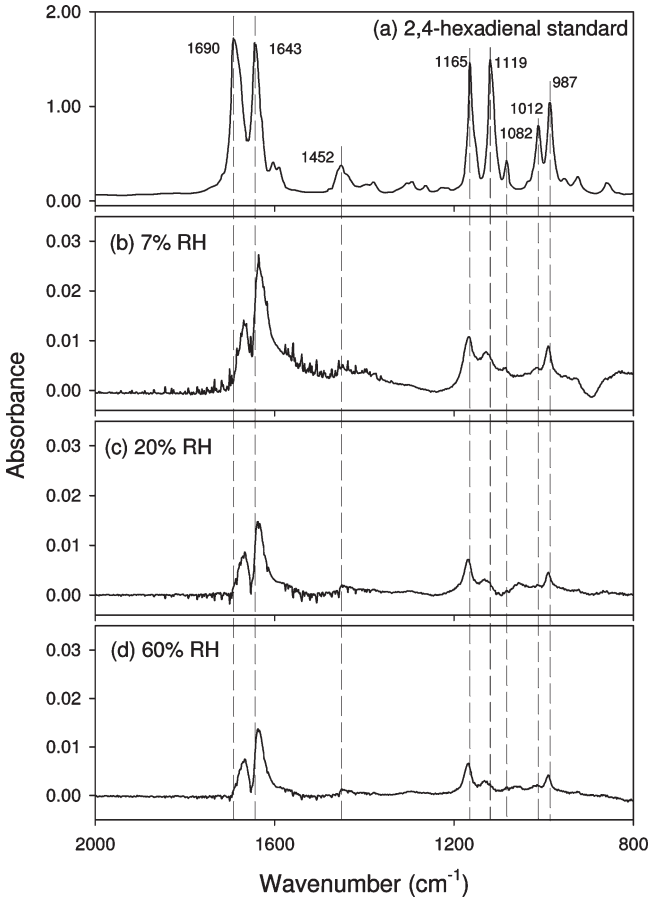

Figure 3. (a) ATR-FT-IR spectra of liquid 2,4-hexadienal standard from the NIST Chemistry WebBook. ATR-FT-IR spectra of the H_2SO_4 film exposed to 2,4-hexadienal at different relative humidity for 15 min: (b) 7% RH; (c) 20% RH; (d) 60% RH.

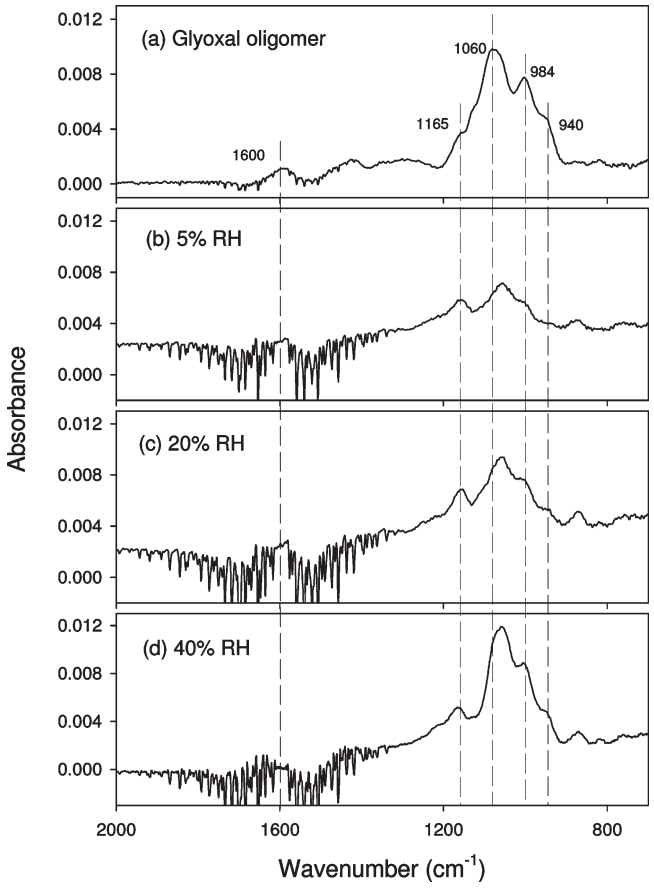

Figure 4. (a) ATR-FT-IR spectra for glyoxal oligomer formed by applying 700 μL of glyoxal trimer dihydrate solution (8.2×10^{-3} M) onto the ATR crystal and evaporating H_2O from the droplet. ATR-FT-IR spectra of the H_2SO_4 film exposed to glyoxal at different relative humidity for 30 min: (b) 5% RH; (c) 20% RH; (d) 40% RH.

the intensity of those characteristic aldol peaks decreased and reached a constant value after ~40 min. For example, the height of the 1165 cm^{-1} band decreased by 53%, 60%, and 30% respectively at 7%, 20%, and 60% RH after termination of the exposure, indicating that 2,4-hexadienal uptake is partially reversible.

The three ATR-FT-IR spectra in Figure 4b–d for H_2SO_4 particles upon exposure of glyoxal at different relative humidity are similar to that of glyoxal oligomer (Figure 4a) formed by depositing 700 μL of glyoxal trimer dihydrate solution (8.2×10^{-3} M) on the ZnSe crystal and evaporating H_2O, with the 1165 cm^{-1} band being more prominent and the 1060 cm^{-1} band shifting to a lower frequency. Those observations confirm that glyoxal oligomers are formed on H_2SO_4 particles. We attribute the 940 cm^{-1} band to an asymmetrical C–O–C stretch of glyoxal oligomers linked by 5-membered dioxolane rings, the 984 and 1165 cm^{-1} bands to the presence of glyoxal trimer dihydrate with unknown structure, the 1060 cm^{-1} band to the C–OH stretch, and the broad 1600 cm^{-1} band to liquid H_2O.[37,40] The 1165 cm^{-1} band likely represents the absorption of dialkyl sulfate ester[37] that has been observed in a previous aerosol mass spectrometry study.[41] The red shift of the C–OH stretch (1060 cm^{-1}) in Figure 4b–d is due to the formation of hydrogen bond between the oxygen atom in the C–OH group and the proton from sulfuric acid, which lengthens the C–OH bond distance and decreases the corresponding force constant of the harmonic oscillation (see Scheme 1b).[37]

The observed relative intensity of the three spectra (Figure 4b–d) upon glyoxal exposures at different RH is consistent with the dependence of the previously measured growth factor with RH by nano-TDMA; i.e., the glyoxal uptake is stronger at higher RH.[19] The intensity of glyoxal oligomer continued to increase throughout the 60 min exposure time, suggesting no limitation for oligomer formation. After the exposure to glyoxal was terminated, a gradual diminution of the absorption feature from 1200 to 800 cm^{-1} was observed during an additional 60 min monitoring period (not shown in Figure 4), indicating that glyoxal uptake is partially reversible.

4. DISCUSSION

Our results indicate that uptake of alcohols and methylglyoxal on H_2SO_4 nanoparticles is significantly different from that on bulk solutions.[30,35] The gas–particle interaction is determined by gas-phase diffusion, mass accommodation, and liquid-phase diffusion and reaction. The occurrence of the particle-phase reaction is related to the concentrations of the organic vapors and the particle residence time. In our present experiments, the gaseous concentrations of organic vapors are higher (10^{12}–10^{16} molecules cm^{-3}) than those in the atmosphere, but a shorter

Scheme 1

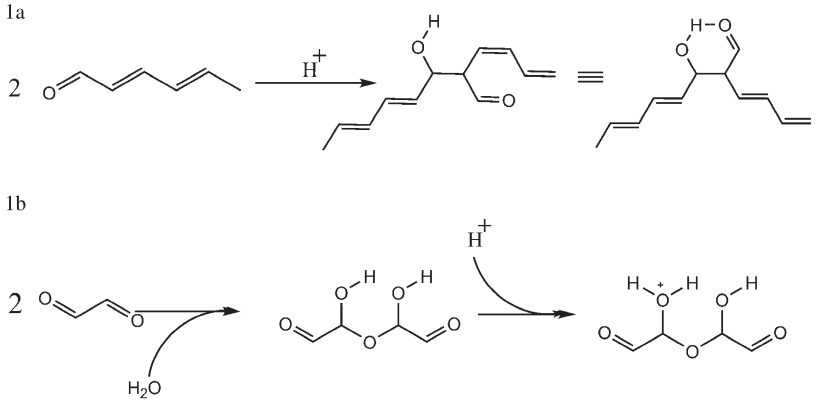

gas−particle interaction time (about 30 s) is employed. For comparable acidity and temperature, the measured negligible growth of alcohols and methylglyoxal on H_2SO_4 nanoparticles is in contrast to the noticeable reversible or irreversible uptake of those species on bulk H_2SO_4 solutions, even if the gaseous concentrations are 1−4 orders magnitude higher in the present work than those in the previous experiments.[30,35] We conclude that for nanoparticles the rate-liming step in the heterogeneous reactions corresponds to mass accommodation, i.e., incorporation of organic species into nanoparticles. Those organic species are sufficiently volatile, and their partitioning is highly suppressed because of the curvature effect, leading to negligible aqueous concentrations of the organics and hindrance in heterogeneous reactions on nanoparticles. Hence, the difference in uptake of alcohols and methylglyoxal between bulk solutions and nanoparticles can be jointly explained by their volatility and the curvature effect.

Heterogeneous reactions between alcohols and sulfuric acid have been suggested to be unlikely of importance in the lower atmosphere except in the case of freshly nucleated aerosols that have high acid concentrations.[35,42,43] In dilute sulfuric acid, alcohols interact with sulfuric acid due to both reversible physical absorption and irreversible reaction, with an increasing Henry's law constant with acidity. In concentrated sulfuric acid, irreversible uptake occurs due to formation of alkyl hydrogen sulfate and/or dialkyl sulfate. Our present study focuses on the uptake of alcohols by H_2SO_4 nanoparticles of relatively high acidity (50−75 wt %) under low RH, suggesting that esterification of alcohols contributes negligibly to the growth of freshly nucleated particles in the atmosphere. Our study is in agreement with the lifetime of alcohols calculated by the reaction rate between alcohols and H_2SO_4 at high acidity, the atmospheric concentrations of alcohols, and the time scale for nucleation growth.[44]

Methylglyoxal has been proposed to be an important precursor of secondary organic aerosol[30,45] because of its large yield from oxidation of biogenic and anthropogenic hydrocarbons.[46,47] Previous measurements indicated that uptake of methylglyoxal on bulk sulfuric acid solutions decreases with acidity in the range of 55−85 wt % and that hydration and polymerization likely explain the measured uptake of methylglyoxal in dilute H_2SO_4.[30] Also, the measurements in bulk liquid H_2SO_4 did not show an acid-catalyzed uptake of methylglyoxal and revealed negligible esterification of methylglyoxal. The lack of nanoparticle growth from exposure to methylglyoxal in the present study indicates a negligible importance of methylglyoxal in growth of freshly nucleated particles in the acid range of 50−75 wt % H_2SO_4. Another previous environmental chamber study showed little growth when $(NH_4)_2SO_4/H_2SO_4$ seed particles with a mean diameter of 80−100 nm were exposed to ∼960 ppb methylgyoxal at ∼50% RH.[48]

In contrast, noticeable nanoparticle growth has been previously measured in the presence of glyoxal, particularly at higher relative humidity, i.e., lower acidity and higher water activity.[19] The similarity in the molecular structure between methylglyoxal and glyoxal cannot explain the difference in their contributions to nanoparticle growth. Secondary organic aerosol formation from gas-phase glyoxal likely occurs by self-oligomerization through hemiacetal formation and/or aldol condensation.[49] The oligomerization process for glyoxal has been proposed to be an acid-catalyzed mechanism, where glyoxal hydration is followed by self-reaction to form cyclic acetal structures.[50−52] Another previous study has suggested that partitioning of glyoxal is controlled by the ionic strength of seed aerosols, rather than the acidity.[48] In the case of methylglyoxal, oligomer formation has been proposed to occur via aldol condensation reactions according to an aerosol mass spectrometer study,[52] in contrast to a hydration and polymerization mechanism from the measurement of methylglyoxal uptake over bulk liquid H_2SO_4 surfaces.[30] Although the exact mechanisms for glyoxal and methylglyoxal self-oligomerization remain an open question, the difference in the heterogeneous reactions of gyloxal and methylglyoxal on nanoparticles may be explained by their different Henry's law constants. The effective Henry's law constant for glyoxal is at least 3 orders of magnitude larger than that of methylglyoxal,[30,48] leading to a much lower aqueous concentration of methylglyoxal in nanoparticles for similar gas phase concentrations of glyoxal and methylglyoxal in our nano-TDMA experiments.

Oligomerization of glyoxal is likely enhanced if nanoparticles contain one or two molecules of low-volatility reactive products formed through a first-order kinetic process,[49] such as formation of diols from hydrolysis of epoxide.[53] By analogy, the presence of pre-existing diols in nanoparticles may also lead to a contribution of methylglyoxal to H_2SO_4 nanoparticle growth by hemiacetal reaction.[49]

Although the nano-TDMA experiments of alcohols suggest that direct esterification by sulfuric acid contributes negligibly to the growth of freshly nucleated particles in the atmosphere, it is plausible that alcohols may react with terminal carbonyl groups

in the pre-existing glyoxal oilgomers to form a hemiacetal product.[49] The chemical composition analysis of glyoxal oligomers suggests the present of the terminal carbonyl group (C═O).[19]

The ATR-FT-IR data demonstrate unambiguous spectroscopic signatures of high molecular weight aldol and oligomer products. Also, desorption of monomers measured in the ATR-FT-IR experiments shows that polymerization and oligomerization reactions of glyoxal and 2,4-hexadienal are partially reversible. This is in contrast to the detection of the products on nanoparticles exposed to the two species using TD-CIMS, implying that the heterogeneous reactions to form oligomers and polymers are largely irreversible.[19]

5. CONCLUSIONS

Combining our present and previous[19] results, we conclude that there are only limited heterogeneous reactions of organics that are important for the growth of nanoparticles. Direct esterification of alcohols and self-oligomerization of methylglyoxal are unlikely to contribute to sulfuric acid nanoparticle growth. Our ATR-FTIR measurements show for the first time spectroscopic evidence of the presence of glyoxal oligomers and 2,4-hexadienal polymers in deposited nanoparticles. Those spectroscopic signatures will be useful for field identification of the nonvolatility organic species in atmospheric nanoparticles.[54] Furthermore, the observed reversibility of heterogeneous reactions of polymerization and oligomerization will have implications in chemical composition analysis of nanoparticles under ambient conditions.

Further experimental studies are needed to identify other organic species that can also enhance nanoparticle growth through heterogeneous reactions. For instance, the reactions between epoxides and sulfuric acid lead to the formation of hydroxy sulfate ester through a pathway similar to diol formation,[53,55] which may occur on nanoparticles. Also, the presence of enormously diverse organic compounds in the atmosphere can lead to synergistic effects in the particle phase. Laboratory experiments suggested that organic acids do not significantly contribute to nanoparticle growth, showing a mass ratio of ~1000 to 1 between H_2SO_4 and *cis*-pinonic acid (CPA) in nanoparticles formed from the H_2SO_4−CPA−H_2O ternary nucleation.[11] Also, recent theoretical and laboratory studies showed that the critical nucleus likely contain only one molecule of organic species.[3,56−58] However, chemical composition analysis of ambient nanoparticles indicated the presence of formate, acetate, and propionate.[23] This discrepancy may be explained by a synergistic effect between organic acids and alkylamines. Furthermore, chemical species may contribute to nanoparticle growth via distinct mechanisms, dependent on their atmospheric abundances. For example, amines may be responsible for nanoparticle growth by neutralization of sulfuric acid or replacement of ammonia, dependent on the relevant abundances between ammonia and amines.[59] Clearly, the complexity of the role of organics in atmospheric nanoparticle growth warrants future research in the laboratory and in the atmosphere to achieve a quantitative understanding of nucleation and growth of nanoparticles and for incorporation of new particle formation in atmospheric models.[3]

AUTHOR INFORMATION

Corresponding Author

*E-mail: renyi-zhang@tamu.edu.

ACKNOWLEDGMENT

This work was supported by the Robert A. Welch Foundation (Grant A-1417) and the US National Science Foundation (AGS-0938352).

REFERENCES

(1) Kulmala, M.; Vehkamäki, H.; Petäjä, T.; Del Maso, M.; Lauri, L.; Kerminen, V. M.; Birmili, W.; Mcmurry, P. H. *J. Aerosol Sci.* **2004**, *35*, 143–176.

(2) Holmes, N. S. *Atmos. Environ.* **2007**, *41*, 2183–2201.

(3) Zhang, R. *Science* **2010**, *328*, 1366–1367.

(4) Benson, D. R.; Young, L. H.; Kameel, F. R.; Lee, S. H. *Geophys. Res. Lett.* **2008**, *35*, L11801 (doi: 11810.11029/12008gl033387).

(5) Sipilä, M.; Berndt, T.; Petäjä, T.; Brus, D.; Vanhanen, J.; Stratmann, F.; Patokoski, J.; Mauldim, R. L., III; Hyvärinen, A.-P.; Lihavainen, H.; Kulmala, M. *Science* **2010**, *327*, 1243–1246.

(6) Ball, S. M.; Hanson, D. R.; Eisele, F. L.; McMurry, P. H. *J. Geophys. Res.* **1999**, *104*, 23709–23718.

(7) Benson, D. R.; Erupe, M. E.; Lee, S. H. *Geophys. Res. Lett.* **2009**, *36*, L15818 (doi: 15810.11029/12009gl038728).

(8) Yu, F. Q.; Turco, R. P. *J. Geophys. Res.* **2001**, *106*, 4797–4814.

(9) Lee, S. H.; Reeves, J. M.; Wilson, J. C.; Hunton, D. E.; Viggiano, A. A.; Miller, T. M.; Ballenthin, J. O.; Lait, L. R. *Science* **2003**, *301*, 1886–1889.

(10) Zhang, R.; Suh, I.; Zhao, J.; Zhang, D.; Fortner, E. C.; Tie, X.; Molina, L. T.; Molina, M. J. *Science* **2004**, *304*, 1487–1490.

(11) Zhang, R.; Wang, L.; Khalizov, A. F.; Zhao, J.; Zheng, J.; McGraw, R. L.; Molina, L. T. *Proc. Natl. Acad. Sci. U.S.A.* **2009**, *106*, 17650–17654.

(12) (a) Solomon, S.; et al. *IPCC Climate Change 2007: The Physical Science Basis*; Cambridge University Press: New York, 2007. (b) Zhang, R.; Li, G.; Fan, J.; Wu, D. L.; Molina, M. J. *Proc. Natl. Acad. Sci. U.S.A.* **2007**, *104*, 5295–5299.

(13) U.S. Environmental Protection Agency. Air quality criteria for particulate matter. EPA 600/P-99/002bF: Research Triangle Park, NC: National Center for Environmental assessment, Office of Research and Development, 2004.

(14) (a) Zhang, R.; Leu, M. T.; Molina, M. J. *Geophys. Res. Lett.* **1996**, *23*, 1669–1672. (b) Molina, M. J.; Molina, L. T.; Zhang, R.; Meads, R.; Spencer, D. *Geophys. Res. Lett.* **1997**, *24*, 1619–1622.

(15) Wehner, B.; Petäjä, T.; Boy, M.; Birmili, W.; Tuch, T.; Wiedensohler, A.; Kulmala, M. *Geophys. Res. Lett.* **2005**, *32*, L17810 (doi: 10.1029/2005GL023827).

(16) Yue, D. L.; Hu, M.; Zhang, R.; Wang, Z. B.; Zheng, J.; Wu, Z. J.; Wiedensohler, A.; He, L. Y.; Huang, X. F.; Zhu, T. *Atmos. Chem. Phys.* **2010**, *10*, 4953–4960.

(17) Seinfeld, J. H.; Pandis, S. N. *Atmospheric Chemistry and Physics: From Air Pollution to Climate Change*; John Wiley: Hoboken, NJ, 2006.

(18) Zhang, K. M.; Wexler, A. S. *J. Geophys. Res.* **2002**, *107*, D21 (doi: 10.1029/2002JD002180).

(19) Wang, L.; Khalizov, A. F.; Zheng, J.; Xu, W.; Ma, Y.; Lal, V.; Zhang, R. *Nature Geosci.* **2010**, *3*, 238–242.

(20) Hirsikko, A.; Laakso, L.; Horrak, U.; Aalto, P. P.; Kerminen, V.-M.; Kulmala, M. *Boreal Environ. Res.* **2005**, *10*, 357–369.

(21) Riipinen, I.; Manninen, H. E.; Yli-Juuti, T.; Boy, M.; Sipila, M.; Ehn, M.; Junninen, H.; Petaja, T.; Kulmala, M. *Atmos. Chem. Phys.* **2009**, *9*, 3317–3330.

(22) Smith, J. N.; Dumn, M. J.; VanReken, T. M.; Iida, K.; Stolzenburg, M. R.; McMurry, P. H.; Huey, L. G. *Geophys. Res. Lett.* **2008**, *35*, L04808 (doi: 10.1029/2007GL032523).

(23) Smith, J. N.; Barsanti, K. C.; Friedli, H. R.; Ehn, M.; Kulmala, M.; Collins, D. R.; Scheckman, J. H.; Williams, B.; McMurry, P. H. *Proc. Natl. Acad. Sci. U.S.A.* **2010**, 6634–6639.

(24) Ehn, M.; Petäjä, T.; Birmili, W.; Junninen, H.; Aalto, P.; Kulmala, M. *Atmos. Chem. Phys.* **2007**, *7*, 677–684.

(25) Laaksonen, A.; et al. *Atmos. Chem. Phys.* **2008**, *8*, 2657–2665.

(26) Wang, L.; Lal, V.; Khalizov, A. F.; Zhang, R. *Environ. Sci. Technol.* **2010**, *44*, 2461–2465.
(27) Zhang, D.; Zhang, R.; Park, J.; North, S. W. *J. Am. Chem. Soc.* **2002**, *124*, 9600–9605.
(28) Suh, I.; Lei, W.; Zhang, R. *J. Phys. Chem. A* **2001**, *105*, 6471–6478.
(29) Zhang, D.; Lei, W.; Zhang, R. *Chem. Phys. Lett.* **2002**, *358*, 171–179.
(30) Zhao, J.; Levitt, N. P.; Zhang, R.; Chen, J.-M. *Environ. Sci. Technol.* **2006**, *40*, 7682–7687.
(31) Fortner, E. C.; Zhao, J.; Zhang, R. *Anal. Chem.* **2004**, *76*, 5436–5440.
(32) Zheng, J.; Khalizov, A. F.; Wang, L.; Zhang, R. *Anal. Chem.* **2010**, *82*, 7302–7308.
(33) Smith, J. N.; Moore, K. F.; McMurry, P. H.; Eisele, F. L. *Aerosol Sci. Technol.* **2004**, *38*, 100–110.
(34) Zhao, J.; Zhang, R. *Atmos. Environ.* **2004**, *38*, 2177–2185.
(35) Levitt, N. P.; Zhao, J.; Zhang, R. *J. Phys. Chem. A* **2006**, *110*, 13215–13220.
(36) NIST Chemistry WebBook (http://webbook.nist.gov/chemistry/).
(37) Pavia, D. L.; Lampman, G. M.; Kriz, G. S. *Introduction to Spectroscopy*; Harcourt Brace College Publishers: Orlando, FL, 1996.
(38) Singh, M.; Zhou, M.; Paul, D. K.; Klabunde, K. J. *J. Catal.* **2008**, *260*, 371–379.
(39) Zhao, J.; Levitt, N. P.; Zhang, R. *Geophys. Res. Lett.* **2005**, *32*, L09802 (doi: 10.1029/2004GL022200).
(40) Loeffler, K. W.; Koehler, C. A.; Paul, N. M.; De Hann, D. O. *Environ. Sci. Technol.* **2006**, *40*, 6318–6323.
(41) Liggio, J.; Li, S.; Mclaren, R. *J. Geophys. Res.* **2005**, *110*, D10304 (doi: 10.1029/2004JD005113).
(42) Timonen, R. S.; Leu, M.-T. *J. Phys. Chem. A* **2006**, *110*, 6660–6666.
(43) Michelsen, R. R.; Staton, S. J. R.; Iraci, L. T. *J. Phys. Chem. A* **2006**, *110*, 6711–6717.
(44) Minerath, E. C.; Casale, M. T.; Elrod, M. J. *Environ. Sci. Technol.* **2008**, *42*, 4410–4415.
(45) Kalberer, M.; Paulsen, D.; Sax, M.; Steinbacher, M.; Dommen, J.; Prevot, A. S. H.; Fisseha, R.; Weingartner, E.; Frankevich, V.; Zenobi, R.; Baltensperger, U. *Science* **2004**, *303*, 1659–1662.
(46) Fan, J.; Zhang, R. *Environ. Chem.* **2004**, *1*, 140–149.
(47) Zhang, R.; Suh, I.; Lei, W.; Clinkenbeard, A. D.; North, S. W. *J. Geophys. Res.* **2000**, *105*, 24627–24635.
(48) Kroll, J. H.; Ng, N. L.; Murphy, S. M.; Varutbangkul, V.; Flagan, R. C.; Seinfeld, J. H. *J. Geophys. Res.* **2005**, *110*, D23207 (doi: 10.1029/2005JD006004).
(49) Lim, Y. B.; Tan, Y.; Perri, M. J.; Seitzinger, S. P.; Turpin, B. J. *Atmos. Chem. Phys. Discuss.* **2010**, *10*, 14161–14207.
(50) Jang, M.; Kamens, R. M. *Environ. Sci. Technol.* **2001**, *35*, 4758–4766.
(51) Liggio, J.; Li, S.; Mclaren, R. *Environ. Sci. Technol.* **2005**, *39*, 1532–1541.
(52) De Haan, D. O.; Corrigan, A. L.; Tolbert, M. A.; Jimenez, J. L.; Wood, S. E.; Turley, J. J. *Environ. Sci. Technol.* **2009**, *43*, 8184–8190.
(53) Minerath, E. C.; Elrod, M. J. *Environ. Sci. Technol.* **2009**, *43*, 1386–1392.
(54) Jang, M.; Czoschke, N. M.; Lee, S.; Kamens, R. M. *Science* **2002**, *298*, 814–817.
(55) Minerath, E. C.; Schultz, M. P.; Elrod, M. J. *Environ. Sci. Technol.* **2009**, *43*, 8133–8139.
(56) McGraw, R.; Zhang, R. *J. Chem. Phys.* **2008**, *128*, 064508 (doi: 10.1063/1.2830030).
(57) Metzger, A.; et al. *Proc. Natl. Acad. Sci. U.S.A.* **2010**, *107*, 6646–6651.
(58) Zhao, J.; Khalizov, A. F.; Zhang, R.; McGraw, R. *J. Phys. Chem. A* **2009**, *113*, 680–689.
(59) (a) Bzdek, B. R.; Ridge, D. P.; Johnston, M. V. *Atmos. Chem. Phys.* **2010**, *10*, 3495–3503. (b) Bzdek, B. R.; Ridge, D. P.; JohnstonM. V. *J. Phys. Chem. A* **2010**, *114*, 11638–11644. (c) Qiu, Q.; Wang, L.; Lal, V.; Khalizov, A. F.; Zhang, R. *Environ. Sci. Technol.* **2011**, *45*, 4748–4755.